Marc Solal, Olli Holmgren, and Kimmo Kokkonen. Design, simulation and visualization of R-SPUDT devices with transverse mode suppression. IEEE Transactions on Ultrasonics, Ferroelectrics, and Frequency Control, accepted for publication.

Design, Simulation and Visualization of R-SPUDT Devices with Transverse Mode Suppression

Marc Solal, *Member, IEEE*, Olli Holmgren and Kimmo Kokkonen

Abstract— When designing narrow band resonant SPUDT devices, the excitation of undesired transverse modes may result both in extra ripple in the passband and in spurious response in the stop band. To avoid these issues, it was proposed to use an approach similar to the one used for bulk-acoustic-wave devices. The principle is to add a low velocity region at the edge of the transducer. If this edge region is properly designed, the transducer supports a so-called "piston mode", i.e., a mode having a flat transverse amplitude profile across the aperture.

A P-matrix model is extended to account for transverse modes in SPUDTs. The model is used to analyze both regular and piston mode devices. Different physical possibilities to implement the low velocity region are investigated and compared. In particular, it was found important to design the transducer so that the acoustical sources and reflectors extend into the edge region to minimize the coupling to higher order modes. From these considerations, a new implementation for piston mode devices is proposed and demonstrated on a GSM base station 199 MHz filter. Electrical measurements as well as acoustical wave fields measured with an optical interferometer are analyzed and compared to simulations.

***Index Terms*—SPUDT, transverse modes, piston mode, interferometry**

I. Introduction

The excitation of transverse modes in SAW filters is known to result in spurious responses in the rejection band and-or extra ripple in the passband. The effect on the performance is the largest in the case of narrow band resonant filters on quartz. A usual counter measure is to apodize the transducer in order to match the excitation profile in the aperture to one transverse mode shape (typically the first symmetric mode) in order to excite predominantly this mode [1]. Other approaches include using multiple tracks in order to excite predominantly a chosen mode [2,3] or adjusting the portion of the aperture to be active to cancel the coupling to spurious modes[3,4] Another approach described in [5] in the case of a very wideband filter on Lithium Niobate is to use weighted dummy electrodes.

A similar issue exists for bulk-acoustic-wave (BAW) resonators in which several modes can be excited simultaneously. An efficient way to suppress the spurious modes in BAW resonators is to implement a border region having correct width and acoustical properties. By implementing this "ring", it is possible to change the mode shape to make it almost rectangular. Then, since the mode shape is matched to the excitation, only one mode is excited and spurious modes are suppressed [6].

More recently, Mayer et al. [7] proposed a similar approach for surface-acoustic-wave (SAW) devices. The principle is to reduce the wave velocity at the edge region of the transducer aperture. Then, it is also possible to obtain a so called "piston mode" having an almost rectangular shape. The technique they used to obtain this lower velocity at the edge region consists of adding short-circuited grating having more electrodes per wavelength than the center track.

Even though the analogy between designing piston mode SAW and BAW devices is very strong, some differences exist: Firstly, for BAW devices the excitation region includes the edges while it does not for SAW when using the technique described in [7]. Secondly, an important effect when analyzing wave guiding in SAW devices is the varying reflectivity in the different regions. This does not exist for BAW devices.

Besides the method proposed by [7], there are other possibilities to implement the low velocity edges, such as increasing the metal thickness, adding a dielectric overlay or increasing the mark-to-pitch ratio. These techniques allow the extension of the sources and the reflectors in the edge region.

To model transverse modes, a scalar approximation of the wave is generally sufficient [8-11]. A specific problem for SAW devices is the presence of reflectors inside the device. This was addressed in [12] by using a 2D version of the COM model. Later, P matrix based models were developed to account for the non uniform profile of the reflectivity in the transverse direction [13-14]. In this work, the model presented in [14] was extended to handle single-phase-unidirectional-transducer (SPUDT) devices. It was used to compare edge designs (with and without sources) for a 199 MHz GSM base

Manuscript received …, 2008
M. S. is with TriQuint Semiconductor, Apopka, Florida, USA
e-mail: marc.solal@ tqs.com.
O. H. and K.K. are with Helsinki University of Technology
Espoo, Finland

station filter. As a result, a new way to realize piston mode SAW devices is proposed. To confirm this piston mode design, electrical measurements as well as acoustical fields measured with the optical interferometer [15], are analyzed and compared to simulation.

II. PRINCIPLE OF SAW PISTON MODE DEVICES

A. Width of the edge region

Figure 1 illustrates the simplified principle of piston mode devices. The center region of the active aperture (region 1) has a lower velocity than the busbars (region 3) resulting in waveguiding. The edge region (region 2) is designed to have a velocity lower than that in the center region. The end gaps between the fingers and the busbars are neglected at this stage, but are included later in the numerical simulations. Under these conditions, it is possible for the transverse wave vector $k_{y,1}$ to be zero in the region 1. The transverse wave vector is then imaginary (evanescent wave) in the region 3 and real in the region 2.

Using a scalar model for the waves and applying the continuity of the amplitude and its y derivative as boundary conditions, it is straightforward to express the conditions to allow a mode to propagate with $k_{y,1} = 0$. Assuming the parabolic approximation [16] is valid for the slowness curves and small velocity differences between the regions, the following expression is obtained:

$$\frac{Wf}{v_x} \cong \sqrt{1+\gamma}\,\frac{\arctan\left(\sqrt{-\frac{\Delta_m}{\Delta_g}}\right)}{2\pi\sqrt{-2\Delta_g}} \quad . \qquad (1)$$

In (1), W is the width of the edge region, γ is the anisotropy coefficient and the velocities are:

$$v_m = v_x\left(1+\Delta_m\right) \qquad v_g = v_x\left(1+\Delta_g\right)$$

where v_m is the metallized velocity, i.e. the velocity in the busbars (region 3 in Fig. 1), v_x is the velocity in the center region (region 1) and v_g is the velocity inside the edge region (region 2).

According to (1), the optimal edge width is independent from the width of the region 1 and depends only on the anisotropy and velocities in the different regions. Therefore, the same edge width can be used independently of the transducer aperture. The piston mode can be obtained with a relatively small edge width. For example, for $\Delta_m = -\Delta_g = 10^{-3}$ and $\gamma = 0.38$, the edge width is only 3.2 wavelengths.

In the case of our quartz devices, it was found that the effect of the gaps at the edges of the electrodes is small. However, the edge width is slightly adjusted later when the gap is included in the model.

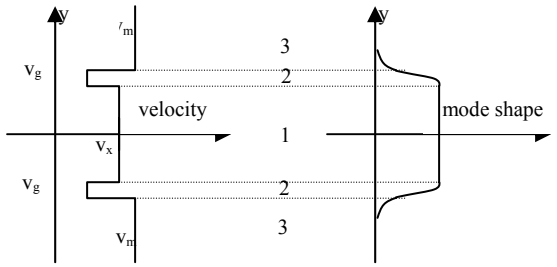

Fig. 1. Simplified velocity profile and mode shape for the piston mode device.

B. SAW specific characteristics for piston mode operation

When trying to apply a piston mode technique to a R-SPUDT [17] design, one difficulty is to determine the grating velocity v_x used in (1). A typical R-SPUDT design includes several regions with different periods. Typically, when using standard electrode-width-controlled (EWC) or distributed-acoustic-reflection-transducer (DART) cells, the device contains some regions having reflectors only, i.e., with half a wavelength period, some regions having sources only, i.e., having a quarter wavelength period and regions having one reflector and one source per wavelength. All these regions have different velocities. As shown in (1), the correct width of the edge region is very sensitive to the velocity differences between the edge region, the center region and the busbars. Therefore, the transversal modes are expected to be different in different regions along the wave propagation direction of the R-SPUDT device.

To illustrate this, Fig. 2 depicts the transversal mode shapes simulated for the different regions of a 199 MHz DART SPUDT filter on Y+36 degrees quartz with a metal thickness of 2500 Å. In this case, the velocities are 3141.09 m/s for the reflector regions and 3136.59 m/s for the source regions. The velocity in the busbars is 3146.7 m/s. The anisotropy coefficient is 0.36. The edge velocity is 3140.99 m/s in the reflector regions and 3133.96 m/s in the source regions. The edge velocity is computed assuming the edge is implemented by increasing the mark to pitch ratio (see below). The edge width is chosen such that a piston mode is obtained when the velocity of the center region is equal to the average of the source velocity and the reflector velocity. Then the calculated mode shape is close to rectangular (solid line in Fig. 2). When computing the mode shapes using velocities corresponding to reflector and source regions, however, the mode shape is not rectangular. In the source region (dotted line), the energy of the main mode is concentrated near the edges, whereas in the reflector region (dashed line), the mode has a cosine-like shape.

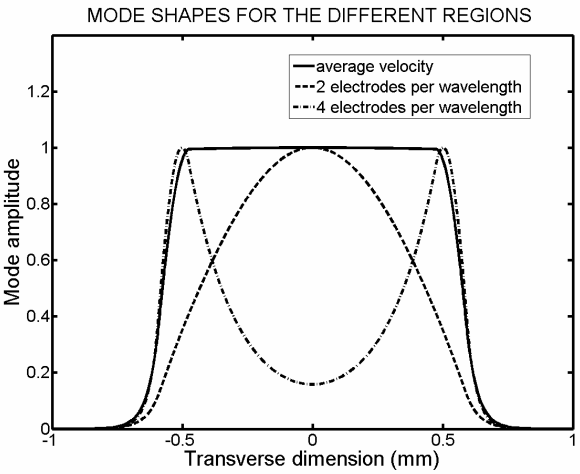

Fig. 2. Transversal mode shapes simulated for the different regions of a 199 MHz DART SPUDT filter with constant edge width. The solid curve corresponds to a center region having a velocity equal to the average of two electrodes per wavelength and four electrodes per wavelength while the dashed and dotted curves correspond to the regions with two and four electrodes per wavelength, respectively.

III. SPUDT DEVICE ANALYSIS

A. General presentation of the model

In [14], a model of SAW devices including both a discrete number of guided modes and a continuum of propagating waves was presented. The model takes into account also the effect of the reflectors limited aperture.

The principle is only recalled briefly here. The first step of the method is to derive the guided modes and continuum. Our model allows us to analyze the case of a symmetric structure comprising 2N+1 regions of different velocities. The parabolic approximation is used to take into account for the crystal anisotropy. To simplify the theory, a scalar approximation is used for the waves. The wave vector component k_x in the propagation direction is the same in all the regions while the wave vector component k_y in the transverse direction is, for each region, derived from the slowness curve. At each interface between two regions, the wave amplitude and its transverse derivative are assumed continuous. By applying these boundary conditions and assuming an evanescent wave (imaginary k_y) in the external regions, the discrete guided modes velocities and shapes are derived. In the case when k_y is real in the external medium, a continuum of waves is found. This continuum is sampled with a fixed increment in k_y.

The second step of the method is to derive the multimode P matrix for one period of the transducer.

$$\begin{bmatrix}[I]\\ [b_L]\\ [b_R]\end{bmatrix}=\begin{bmatrix}[M_{11}] & [M_{12}] & [M_{13}]\\ [M_{21}] & [M_{22}] & [M_{23}]\\ [M_{31}] & [M_{32}] & [M_{33}]\end{bmatrix}\cdot\begin{bmatrix}[V]\\ [a_L]\\ [a_R]\end{bmatrix} \tag{1}$$

Here N_e electrical ports and $2N_m$ acoustical ports are considered, where N_m is the number of discrete modes plus the number of continuum samples. The P matrix relates the N_e voltages *V*, the N_m incoming wave amplitudes at the left side a_L and the N_m incoming wave amplitudes at the right side a_R to the N_e currents *I*, the N_m outgoing wave amplitude on the left side b_L and the N_m outgoing amplitude on the right side b_R. The block M_{11} is the admittance matrix, the blocks M_{22} and M_{33} are the acoustical reflection matrices on the left and right sides. M_{32} and M_{23} are the acoustical transmission matrices. The blocks M_{21} and M_{31} are the electroacoustic coupling matrices while the blocks M_{12} and M_{13} are the acoustoelectric coupling matrices.

As described in [14], the reflection occurs only in the portion of the aperture where the reflector is present. For example there is no reflection in the busbars or on the free surface. This means that the amplitude of the reflected wave is proportional to the amplitude of the incoming wave multiplied by a gating function.

If $g_i(y)$ is the amplitude of the i[th] mode normalized such that $\int|g_i(y)|dy=1$, the reflected wave amplitude at the center of the electrode is :

$$\begin{aligned} rect(y).g_i(y) &= \sum_j R_{ij}g_j(y)\\ R_{ij} &= \int rect(y)g_i(y)g_j^*(y)dy \end{aligned} \tag{2}$$

where *rect*(*y*) is a function defined to be equal to the unity in the reflective region and to zero in the non reflective regions.

Based on these considerations, the scattering part of the P matrix can be derived. If the phase of the mode (or continuum sample) *i* under the period is φ_i and the reflection and transmission coefficients on the electrode are $\sin\Delta$ and $\cos\Delta$, the expressions of the acoustical scattering blocks are:

$$\begin{aligned} M_{22}^{ij} &= M_{33}^{ji} = -j\sin\Delta R_{ji}\exp\left(-j\frac{\varphi_i+\varphi_j}{2}\right)\\ M_{23}^{ij} &= M_{32}^{ji} = \left((\cos\Delta-1)R_{ji}+\delta_{ij}\right)\exp\left(-j\frac{\varphi_i+\varphi_j}{2}\right) \end{aligned} \tag{3}$$

The acoustoelectric and electroacoustic blocks are obtained by computing the mode expansion of the rectangular source of aperture W_j corresponding to the electrical port *j*.

$$P_{ij} = \int_{W_j} g_i^*(y)dy$$

$$M_{12}^{ji} = M_{13}^{ji} = -j\sqrt{Ga}.P_{ij}\exp\left(-j\frac{\varphi_i+\Delta}{2}\right) \quad (4)$$

$$M_{21}^{ij} = M_{31}^{ij} = j\sqrt{Ga}.P_{ij}^*\exp\left(-j\frac{\varphi_i+\Delta}{2}\right)$$

In the previous expression, Ga is the radiation conductance of one electrode.

In the simple case of one track devices, the admittance M_{11} is given by $G_a + jH(G_a)$ where H stands for the Hilbert transform.

The next step of the method is to cascade the P matrix of the consecutive cells. For the case of a DART or EWC device, two different kinds of cells have to be considered: the reflective cells and the transducer cells. In the transducer cells (four electrodes per wavelength), there is no reflectivity ($\Delta = 0$). In this case, the expressions for the acoustical scattering blocks are greatly simplified. The reflection block matrices are simply zero while the transmission block matrices are diagonal matrices:

$$M_{23}^{ij} = M_{32}^{ji} = \delta_{ij}\exp(-j\varphi_i). \quad (5)$$

The P matrices of several consecutive transducer cells can then be cascaded directly by summing the wave amplitudes for the different sources at the boundaries of the four electrodes per wavelength region. If the electrode connectivities l_{in} are defined to be zero except if the electrode *n* is connected to the electrical port *i*, the expression of the P matrix $\overline{M}$ for the cascade of *N* periods is straightforward:,

$$\overline{M}_{22} = \overline{M}_{33} = 0$$

$$\overline{M}_{23}^{ij} = \overline{M}_{32}^{ij} = \exp(-jN\varphi_i)\delta_{ij}$$

$$\overline{M}_{12}^{ij} = -j\sqrt{G_a}P_{ij}\sum_{n=1}^{N} l_{in}.\exp\left(-j\left(n-\frac{1}{2}\right)\varphi_j\right)$$

$$\overline{M}_{13}^{ij} = -j\sqrt{G_a}P_{ij}\sum_{n=1}^{N} l_{in}.\exp\left(-j\left(N-n+\frac{1}{2}\right)\varphi_j\right)$$

$$\overline{M}_{21}^{ji} = j\sqrt{G_a}P_{ij}^*\sum_{n=1}^{N} l_{in}.\exp\left(-j\left(n-\frac{1}{2}\right)\varphi_j\right)$$

$$\overline{M}_{21}^{ji} = j\sqrt{G_a}P_{ij}^*\sum_{n=1}^{N} l_{in}.\exp\left(-j\left(N-n+\frac{1}{2}\right)\varphi_j\right)$$

$$\overline{M}_{11}^{ij} = G_a\sum_{n=1}^{N}\sum_{\substack{m=1\\m\neq n}}^{N} l_{in}l_{jm}\sum_{k=1}^{Nm} P_{ik}P_{jk}^*\exp(-jn\varphi_k) +$$

$$\delta_{ij}(G_a + jB_a)\sum_{n=1}^{N} l_{in} \quad (6)$$

To reduce the computation time, the four electrodes per wavelength regions are detected and treated at once using (6). The reflectors are cascaded period by period.

B. Mode conversion between the different regions

Due to the results shown in Fig. 2, it was assumed it was very important to account for the difference in the mode profiles between the reflective (two electrodes per wavelength) and transductive (four electrodes per wavelength) regions. This difference in mode shapes results in conversion at the boundary between the regions. To analyze this conversion, the two sets of mode shapes $g^{(2)}(y)$ and $g^{(4)}(y)$ and phases $\varphi^{(2)}$ and $\varphi^{(4)}$ for two and four electrodes per wavelength, respectively, are computed. Then, the P matrices are derived as described above for the corresponding modes. The two electrodes per wavelength modes are chosen as the base for the device P matrix.

So, for each transductive region, the P matrix in the four electrodes per wavelength base is computed using (6). The next step is to convert this P matrix to a new matrix on the two electrodes per wavelength modes.

$$\begin{aligned}
&\overline{M}_{12}^{(2)} = \overline{M}_{12}^{(2)}.A \qquad && \overline{M}_{12}^{(2)} = \overline{M}_{12}^{(2)}.A \\
&\overline{M}_{13}^{(2)} = \overline{M}_{13}^{(2)}.A \qquad && \overline{M}_{13}^{(2)} = \overline{M}_{13}^{(2)}.A \\
&\overline{M}_{21}^{(2)} = \widetilde{A}.\overline{M}_{21}^{(4)} \qquad && \overline{M}_{21}^{(2)} = \widetilde{A}.\overline{M}_{21}^{(4)} \\
&M_{22}^{(2)} = M_{33}^{(2)} = 0 \\
&M_{23}^{(2)} = M_{32}^{(2)} = \widetilde{A}.M_{23}^{(4)}.A
\end{aligned} \quad (7)$$

The matrix *A* represents the conversion between the two sets of modes (each one assumed to be orthogonal):

$$A_{i,j} = \int g_i^{(2)}(y)g_j^{(4)^*}(y).dy \quad (8)$$

Since the number of modes may be different for the two electrodes per wavelength regions and the four electrodes per wavelength regions, *A* may not be a square matrix and cannot always be inverted. $\widetilde{A}$ stands for the pseudo inverse of *A*.

One has to notice that this expression is valid for the guided modes only. A correct expression to represent the conversion for the continuum was not found. The reason is that this would probably be possible only by considering reflected waves at the boundary between two different regions.

The model described above is straightforward to implement. The P matrix of a complete device is computed by cascading the individual P matrices (defined for the two electrodes per wavelength modes).

To compute the wave amplitude fields, an additional step has to be performed. After cascading the P matrices, the output wave for given load and source impedances are known on the boundary of the structure. Then, the amplitude fields are computed by multiplying the transfer matrices.

IV. Device Implementation

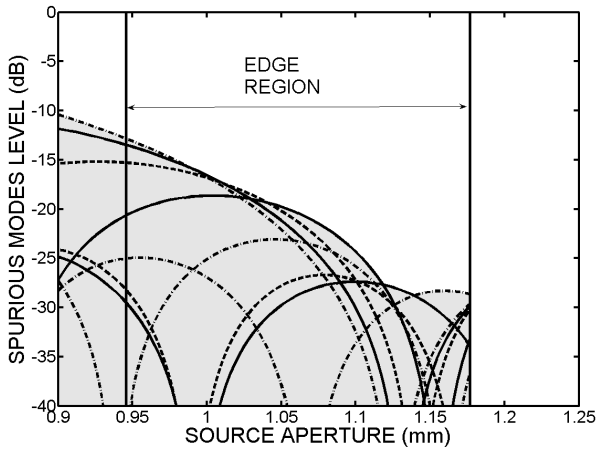

Fig. 3. Estimated relative levels of several spurious modes as a function of the source aperture. The left vertical line corresponds to the center region width while the right line corresponds to the total aperture of the center region and the two edge regions. The points between the two vertical lines correspond to sources extending inside the edge regions. The levels are normalized to the level of the main mode. The estimated overall spurious level as a function of the source aperture is thus obtained as an envelope of all the lines (marked with gray).

The devices described in [7] used short-circuited gratings having a large number of electrodes per wavelength in the edge regions allowing for a reduction in the wave velocity. In their approach, the sources do not extend in the edge region. To study the effect of extending the sources to the edge region, relative levels of spurious modes were estimated with varying source widths for the configuration described in section IIB. This estimation is done by computing the integral of the mode shapes on the source aperture relative to the integral of the main mode. Fig. 3 shows an example of estimated relative levels of numerous spurious modes and the overall level as their envelope as a function of the source aperture. The same geometry is used for all points of the curve, and only the source aperture (i.e., the integration bounds) is varied. The lowest spurious levels are obtained when the sources extend far in the edge region, almost to the boundary between the edge region and the busbar. For example, if the widths of the center and edge regions are 0.945 mm and 0.115 mm, the optimum width of the sources is 1.14 mm. In this case, the expected relative spurious level generated by the transducer is reduced by ~17 dB compared to the case where the sources do not extend to the edge region. Obviously, this effect may become less important if the velocity difference between the regions increases.

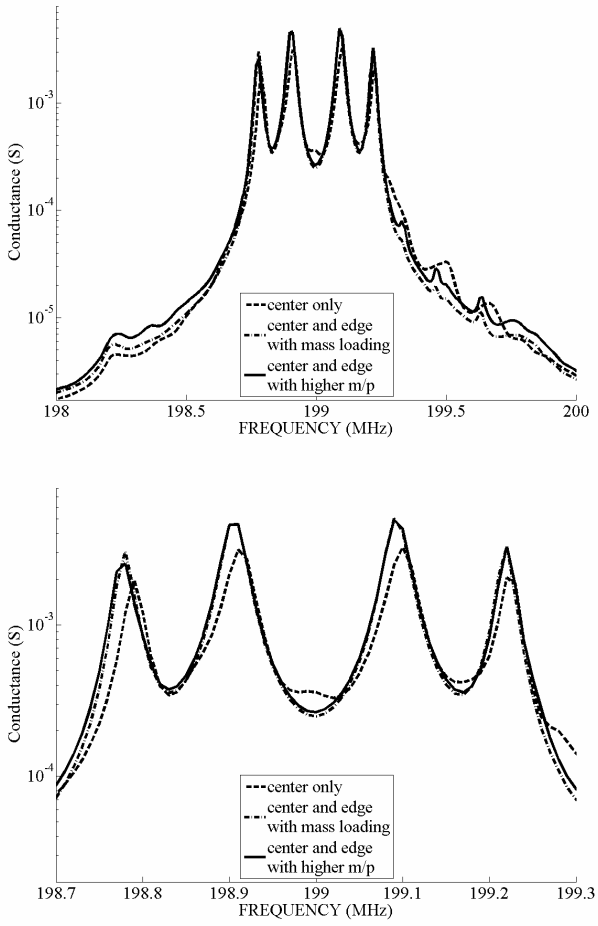

Fig. 4. Simulated conductance for different implementations of the piston mode device without impedance matching: reflectors and source extend in the center region only (dotted line), reflectors and sources extend both in the center and the edge region with mass loading (dashed line) and with higher mark to pitch ratio (*m/p*) (solid line). The four main peaks are due to longitudinal main modes. The spurious modes are seen as additional smaller peaks between the main modes and above the passband. Overall response (top) and zoomed view of the passband (bottom).

To confirm this effect, Fig. 4 shows the simulations results obtained for the same filter for three different implementations of the piston mode device. The best results are obtained when the sources and reflectors extend both in the center and the edge regions. This configuration could be implemented by reducing the velocity in the edge region by increasing its metal thickness or adding a dielectric overlay, i.e., with mass loading (dashed line in Fig. 4). However, it was decided to stay with the one metal layer process and so to increase the mark to pitch ratio (*m/p*) in the edge region. This approach allows both to lower the velocity of the edge region and to extend the sources to the edge region. The split finger width was increased from $\lambda/8$ to $3\lambda/16$ and the reflector width was increased to get constant gaps, see Fig. 5. The simulation of this configuration is shown in solid line in Fig. 4. The improvement when comparing with the initial piston mode configuration, in dotted line, is obvious.

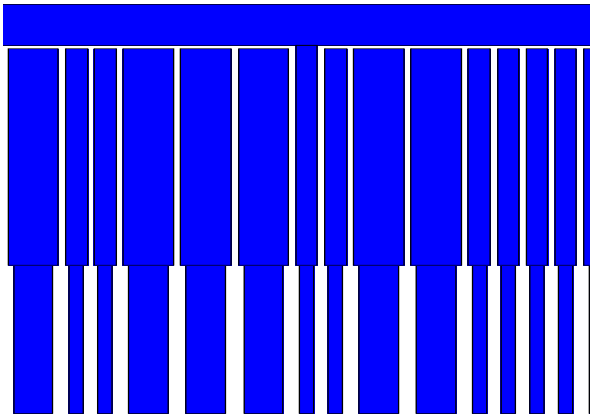

Fig. 5. Detailed view showing the edge region of the implemented piston mode device using higher mark-to-pitch-ratio electrodes. The dark regions correspond to the electrodes. The period of the wide electrodes is half a wavelength while it is a quarter wavelength for the narrow electrodes.

V. Experimental Results

A. Measured electrical responses

Two versions of the same basic filter design were manufactured: a standard device without the edge region and a piston mode device with the edge region. The edge regions with constant width were implemented using higher mark-to-pitch ratio. To choose the width of the edge region, the average of the velocities in the two electrodes per wavelength and in the four electrodes per wavelength was assumed. The expression (1) was used as a first trial. Then, the actual mode shapes were computed by using the numerical method and the edge width was slightly adjusted in order to get a flat transverse profile in the center region.

Figures 6 and 7 show the measured and simulated transfer functions obtained for the standard and piston mode devices, respectively. Both devices were matched to 50 Ω. Due to the narrow relative passband, the minimum insertion is 4 dB for the standard device while it is about 4.8 dB for the piston mode device. The device is also strongly resonant, meaning that the reflections inside the transducers as well as the reflections between the two transducers allow to increase the impulse response duration. The standard device has strong ripple in the pass band due to the transverse modes as well as spurious on the high frequency. Using the edge region, this ripple was reduced from 1.5 dB to about 0.2 dB. This demonstrates the efficiency of the piston mode operation to reduce the effect of the transverse modes.

B. Comparison of the measured and simulated electrical responses

Two sets of simulations are shown in Figs. 6 and 7. The first one (labeled "without conversion" in the figures) uses the average velocities of the four and the two electrodes per period regions to compute the modes everywhere. In this case, there is no difference in the mode shapes in the different regions and no conversion has to be accounted for. The second simulation (labeled "with conversion") takes into account the different mode shapes in the different regions. Despite the very large difference in mode shapes, both simulations give very similar results. This indicates that the average velocity in the center region is a good approximation when computing the width of the edge region and the mode shapes for both the reflective and transductive regions. When the average velocity is used, the continuum can be taken into account.

The match between measurement and simulation is very good especially for the standard device (Fig. 6.). While there are only slight differences in the passband, the continuum analysis helps to predict more accurately the high frequency sidelobes. For the piston mode device (Fig. 7.), the agreement is also good. The passband ripples are greatly reduced but they can still been seen on the measurement while the simulation predicts that they are completely suppressed.

C. Amplitude profiles

To better understand the electrical results, the acoustic amplitude profiles were measured using a scanning laser interferometer [15]. The interferometer detects mechanical vibrations perpendicular to the sample surface. The spatial resolution of the interferometer is better than 1 μm. It should be noted that amplitudes in areas with different reflectivity, e.g., grating and metal surface, cannot be directly compared since the sensitivity of the interferometer depends on the optical reflectivity of the sample surface.

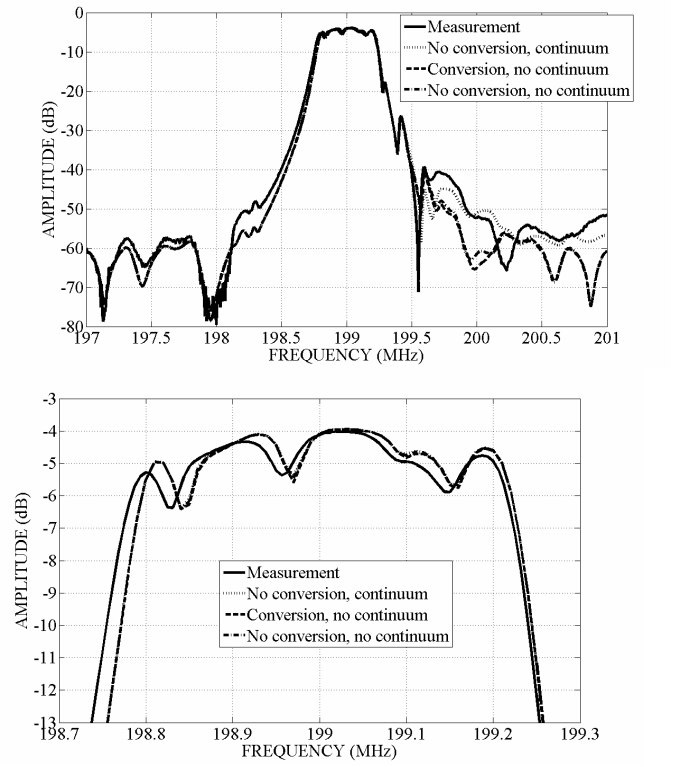

Fig. 6. Comparison between measurement and simulation for the standard device matched to 50 Ω: measurement (solid), simulation without conversion and with continuum (dotted), simulation with conversion and without continuum (dashed), simulation without conversion and without continuum (dash-dotted). No significant difference is found between the results of the simulation with and without conversion. The continuum is explaining the high side rejection. Overall response (top) and zoomed view of the passband (bottom).

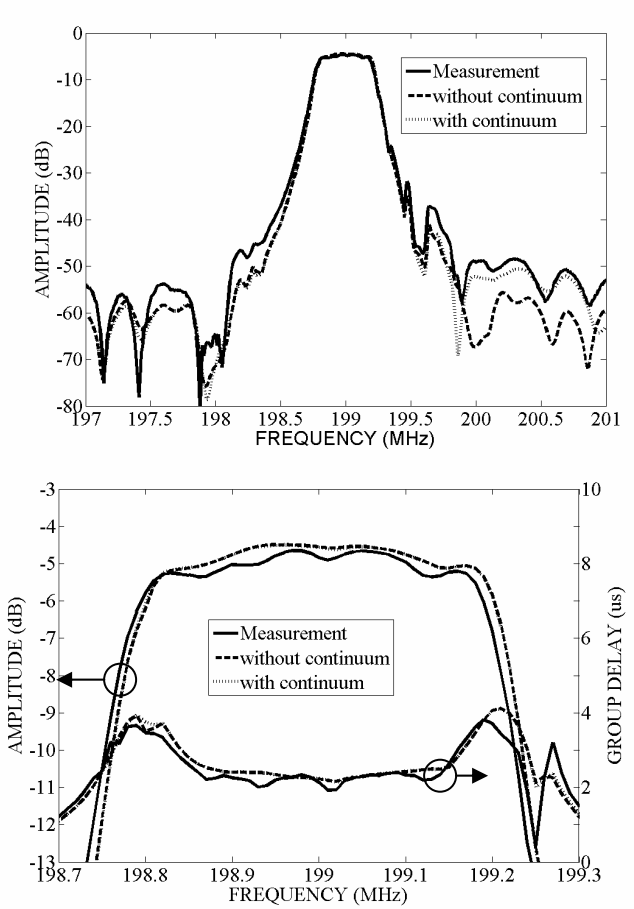

Fig. 7. Comparison between measurement and simulation for the piston mode device matched to 50 Ω: measurement (solid), simulation with conversion and without continuum (dotted), simulation without conversion and with continuum (dashed). Overall response (top) and zoomed view of the passband (bottom).

The interferometer measurements were carried out for 49 frequencies in the frequency range from 198.83 MHz to 199.97 MHz with a frequency step of 0.02 MHz. The dimensions of the measured filters are approximately 10 mm × 1.2 mm, while the finger period in x-direction is relatively small, approximately 4-8 μm. This results in complementary requirements for the scan parameters: the scan step should be small enough to resolve all the details (fingers) while on the contrary the large size of the device would require a large scan step to keep the scan time (and data size) reasonable. In practice, it is not feasible to measure the whole device with high resolution. Therefore, seven smaller scan areas were chosen. Each scan area has 300 x 120 scan points with scan steps of 0.99 μm (x) and 9.90 μm (y), resulting in an area of 297 μm x 1188 μm.

Figures 8-12 show measured and simulated acoustic amplitudes at selected frequencies for the standard and piston mode devices. No impedance matching was used in the measured devices in order to obtain better separation of modes. The simulations assume the average velocity and include the continuum. The frequencies corresponding to the main modes and spurious modes were selected by locating peaks from the electrical responses, measured from the unmatched devices. There is a frequency offset of 0.1 MHz between the measured and simulated frequency responses. The dashed rectangles in the simulated amplitude images indicate the locations corresponding to the measured scan areas. In general, the simulation predicts well the distribution of the acoustic amplitudes in both devices.

Figure 8 compares the measured and simulated amplitude distributions in the standard device (without the edge design) for one of the main modes. The mode shape is smooth and round in y direction, as expected. Figure 9 shows the corresponding mode in the piston mode device (with the edge design). In this case, the transversal mode shape is close to rectangular.

Figure 10 depicts measured and simulated amplitude distribution at the frequency of a spurious mode existing in the standard device. In the figure, the transversal mode structure is clearly visible. Figures 11 and 12 show the amplitude distributions for higher-order modes above the passband for the standard and piston mode devices, respectively.

To illustrate the effect of the edge design to the transverse amplitude profiles more clearly, Figs. 13 and 14 show the measured and simulated transversal amplitude profiles for the main mode shown in Figs. 8 and 9. The measured amplitude profile was obtained by averaging all the lines of the scanned area between x = 2.5 mm and x = 2.8 mm. In addition, the simulated curve was shifted such that the maximum values of the measured and simulated curves coincide. The correspondence is very good for the standard device in Fig. 13. The discontinuities in the measured profiles are due to the difference of optical reflectivity between the transducer and the busbar. For the piston mode device in Fig. 14, the measured profile is slightly less rectangular than predicted by the model. This indicates that the velocity in the edge region is probably slightly underestimated. This would also explain why some transverse mode effect is seen on the electrical filter response.

VI. Conclusion

A new approach to design "piston mode" R-SPUDT devices is proposed. Different physical possibilities to implement the low velocity region enabling piston mode operation were investigated. By extending the sources in the edge regions, a reduction of spurious mode levels is obtained. For a GSM base station 199 MHz filter considered here, the passband ripple due to the transverse spurious modes was reduced from 1.5 dB to about 0.2 dB. Experimental results of both electrical responses and acoustical amplitude fields are presented validating both the simulations and the successful application of the new design concept.

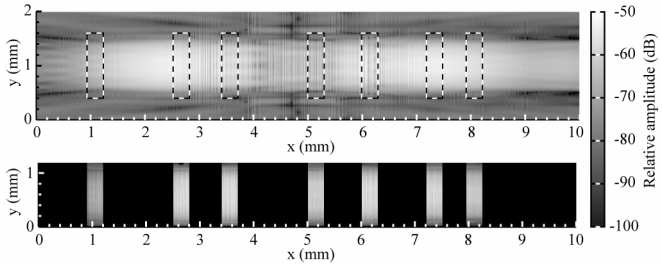

Fig. 8. Acoustic wave fields in the standard device without the edge design for one of the main modes: simulation at 198.915 MHz (top), measurement at 199.01 MHz (bottom).

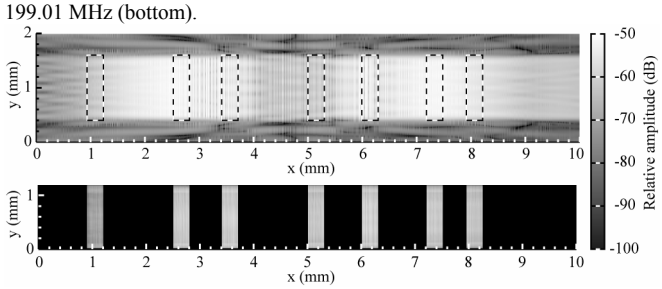

Fig. 9. Acoustic wave fields in the piston mode device with the edge design for one of the main modes: simulation at 198.91 MHz (top), measurement at 199.01 MHz (bottom)

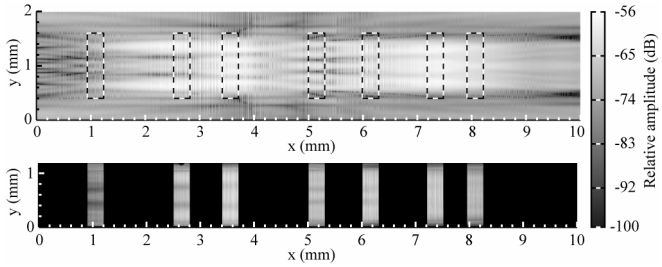

Fig. 10. Acoustic wave fields in the standard device for a spurious mode: simulation at 198.975 MHz (top), measurement at 199.07 MHz (bottom)

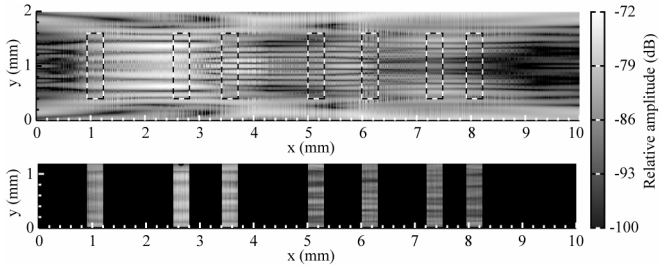

Fig. 11. Acoustic wave fields in the standard device above the passband: simulation at 199.695 MHz (top), measurement at 199.79 MHz (bottom)

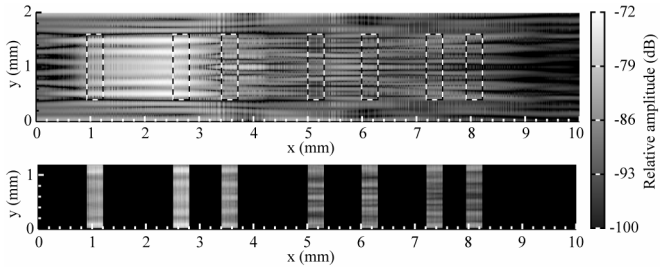

Fig. 12. Acoustic wave fields in the piston mode device above the passband: simulation at 199.69 MHz (top), measurement at 199.79 MHz (bottom).

ACKNOWLEDGMENTS

O.H. and K.K. thank the Alfred Kordelin Foundation, the Finnish Cultural Foundation and the Nokia Foundation for scholarships.

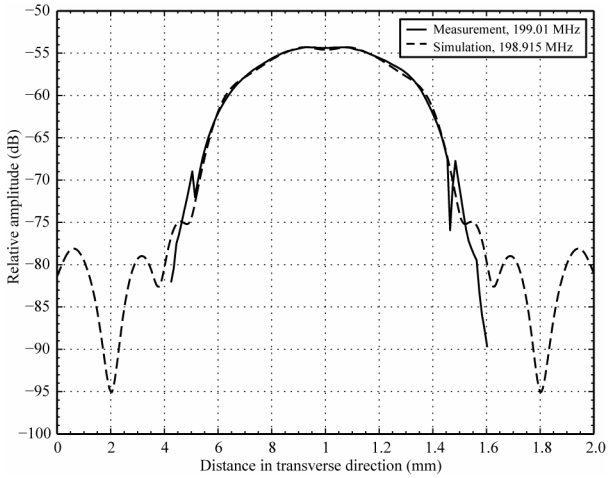

Fig. 13. Comparison between the measured and simulated transverse profile of the acoustic amplitude for the standard device at x=2.65mm. The discontinuities on the measured curve are due to the difference in optical reflectivity between the busbars and the transducer.

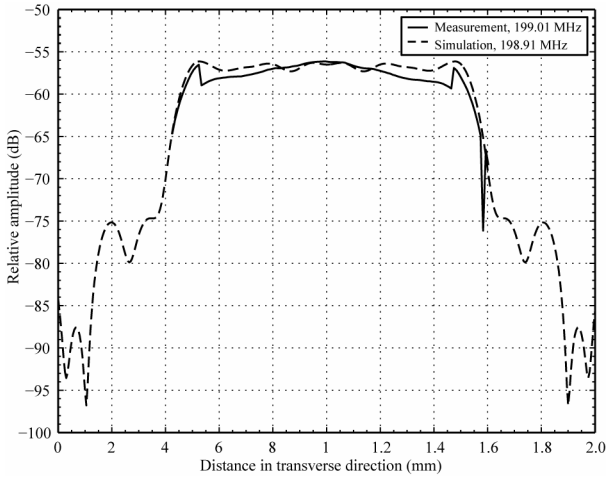

Fig. 14. Comparison between the measured and simulated transverse profile of the acoustic amplitude for the piston mode device at x=2.65mm. The discontinuities on the measured curve are due to the difference in optical reflectivity between the busbars and the different regions of the transducer.

REFERENCES

[1] S. A. Wilkus, C. S. Hartmann, and R. J. Kansy, "Transverse mode compensation of surface acoustic wave filters", in Proc. IEEE Ultrasonics Symposium, 1985, pp. 43-47.

[2] G. Martin, B. Wall, and M. Waihnacht, "An alternative method for suppressing undesired transverse modes in longitudinally coupled SAW resonator filters", IEEE Trans. Ultrason., Ferroelect., Freq. Contr. vol. 42, pp. 1099-1101, 1995.

[3] M. Mayer, A. Bergmann, K. Wagner, M. Schemies, T. Telgmann, and A. Glas, "Low resistance quartz resonators for automotive applications without spurious modes," *IEEE Ultrason. Symp.*, 2004, pp. 1326–1329.

[4] Y. Yamamoto and S. Yoshimoto, "SAW transversely guided mode spurious elimination by optimization of conversion efficiency using W/W0 electrode structure", in Proc. IEEE Ultrasonics Symposium, 1998, pp. 229-234.

[5] T. Omori, K. Matsuda, N. Yokoyama, K. Hashimoto, and M. Yamaguchi, "Suppression of transverse mode responses in ultra-

wideband SAW resonators fabricated on a Cu-grating/15YX-LiNbO3 structure", IEEE Trans. Ultrason., Ferroelect., Freq. Contr. vol. 54, pp. 1943-1948, 2007.

[6] J. Kaitila, M. Ylilammi, J. Ella, and R. Aigner, "Spurious resonance free bulk acoustic wave resonators", in Proc. IEEE Ultrasonics symp, 2003, pp. 84-87.

[7] M. Mayer, A. Bergmann, G. Kovacs, and K. Wagner, "Low loss recursive filters for basestation applications without spurious modes," in Proc. IEEE Ultrasonics symp., 2005, pp 1061-1064.

[8] J. K Knowles, "A note on elastic surface waves", Jour. Geophysical Res. vol. 71, pp. 5480-5481, Nov. 15,1966

[9] J. Schoenwald, "Optical waveguide model for SAW resonators", in Proc. IEEE Int. Freq. Contr. Symp., 1976, pp. 340-345.

[10] C. K. Campbell, "Modelling the transverse-mode response of a two-port SAW resonator", IEEE Trans. Ultrason., Ferroelect., Freq. Contr. vol. 38, pp. 237-242, 1991.

[11] G. Clark, R.-F. Milsom, and J. Schofeld, "3-D modal analysis of SAW filters", in Proc. IEEE Ultrasonics Symposium, 1985, pp. 26-31.

[12] H. A. Haus and K. L. Wang, "Modes of grating waveguide", J. Appl. Phys vol. 49, pp. 1061-1069, 1978.

[13] K. Wagner, M. Mayer, A. Bergmann, and G. Riha, "A 2D P-Matrix Model for the Simulation of Waveguiding and Diffraction in SAW Components", in Proc. IEEE Ultrasonics Symp., 2006, pp. 380-388.

[14] M. Solal, V. Laude, S. Ballandras, "A P-Matrix Based Model for SAW Grating Waveguides Taking into Account Modes Conversion at the Reflection", in IEEE Trans. on UFFC, vol. 51, no 12, pp 1690-1696, Dec. 2004.

[15] J. V. Knuuttila, P. T. Tikka, and M. M. Salomaa, "Scanning Michelson interferometer for imaging surface acoustic wave fields," Opt. Lett. vol. 25, pp. 613-615, 2000.

[16] T. L. Szabo and A. Slobodnick, "The effect of diffraction on the design of acoustic surface wave devices," *IEEE Trans. Sonics Ultrason.*, vol. 20, pp. 240–251, Jul. 1973.

[17] P. Ventura, M. Solal, P. Dufilie, J.M. Hode, and F.Roux, "A New Concept in SPUDT Design: the RSPUDT (Resonant SPUDT)" in Proc. IEEE Ultrasonics symp., 1994, pp 1-6.

[18] M. Solal, "A P-Matrix-Based Model for the Analysis of SAW Transversely Coupled Resonator Filters, Including Guided Modes and a Continuum of Radiated Waves", in IEEE Trans. on UFFC, vol 50, no 12, pp 1729-1741, Dec. 2003.